ELSEVIER

International Journal of Solids and Structures 41 (2004) 2879–2898

INTERNATIONAL JOURNAL OF SOLIDS and STRUCTURES

www.elsevier.com/locate/ijsolstr

Characteristics of a crack propagating along the gradient in functionally gradient materials

Kwang Ho Lee *

Department of Mechanical Engineering, Sangju National University, 386 Gajang Dong, Sangju City, Kyungbuk 742-711, South Korea

Received 9 December 2003; received in revised form 9 December 2003

Available online 27 February 2004

Abstract

Stress and displacement fields for a crack propagating along gradient in a functionally gradient material, which has (1) a linear variation of shear modulus with a constant density and Poisson's ratio, and (2) an exponential variation of shear modulus and density under a constant Poisson's ratio, are developed.

The equations of motion in nonhomogeneous materials are first developed using displacement potentials and the solution to the displacement fields and the stress fields for a crack propagating at constant speed though an asymptotic analysis. The influence of nonhomogeneity on the higher order terms of the stress fields are explicitly brought out. Using these stress components, isochromatic fringes around the propagating crack are generated for different crack speeds and nonhomogeneity and the effects of nonhomogeneity on these fringes are discussed.

Keywords: Functionally gradient materials; FGM constant; Propagating crack; Stress and displacement fields; Stress intensity factors

1. Introduction

Several novel materials have recently been developed to meet the increasing demand of modern technology (Niino et al., 1987; Butcher et al., 1999; Jedamzik et al., 2000; Zeng et al., 2000). Among these, functionally graded materials (FGMs) are unique in that they offer the possibility of tailoring their constituents and gradation to match the end use. These materials also have certain advantages over existing isotropic materials and conventional composites, especially in applications that demand, resistance to corrosion and high temperature as in furnace walls and turbine blades, wear resistance as in gears and high speed machine tools, combined with good toughness and strength characteristics. Conventional materials, which satisfy all these requirements, are rare. The general practice therefore has been to provide an interior wall made of high heat resistance material in the case of furnaces and in the case of gears and tools with super wear resistance material. Unfortunately, such interior walls or coatings are mechanically weak at the interface due to discontinuous stresses resulting from thermal gradients and due to poor bond strength,

* Tel.: +82-54-530-5404; fax: +82-54-530-5407.
E-mail address: khlee@sangju.ac.kr (K.H. Lee).

0020-7683/$ - see front matter © 2004 Elsevier Ltd. All rights reserved.
doi:10.1016/j.ijsolstr.2004.01.004

leading to interface cracking and spallation. FGMs can be effectively designed to overcome these deficiencies, by proper choice of the constituents and gradation. The spatial variation of the material composition in FGMs results in a medium with varying elastic and physical properties and calls for special methods of processing and analysis.

Until now, the fracture of an FGM under quasi-static loading, which is one of the predominant modes of material failure, has been investigated extensively (Erdogan, 1995; Jin and Batra, 1996; Gu et al., 1999). The primary conclusion of these investigations is that the classical inverse square root singular nature of the stress field is preserved in FGMs, however, the stress intensity factor is influenced by the nonhomogeneity of the material. Therefore, very close to the crack tip in FGMs, the stresses are identical to that in a homogeneous material. The structure of the stress field away from crack tip is significantly altered by nonhomogeneity, as has been demonstrated by Eischen (1987) and Parameswaran and Shukla (2002).

The behavior of propagating cracks in FGMs has also attracted some attention. Following an earlier study by Atkinson and List (1978), several groups have investigated the behavior of propagating cracks in FGMs especially after their introduction. (Wang and Meguid, 1995; Rousseau and Tippur, 2001; Jiang and Wang, 2002). For propagating cracks along the gradient in FGMs, Parameswaran and Shukla (1999, 2002) developed the structure of the first stress invariant and the out of plane displacement bring out the effects of nonhomogeniety. However, nonhomogeneity specific terms for individual stress components have not been developed. Such stress fields are required in the analysis of full field experimental data obtained through techniques such as photoelasticity and coherent gradient sensing (CGS). This paper provides the stress and displacement fields for a crack propagating at a constant speed along the direction of property variation in an FGM. The elastodynamic problem is formulated in terms of displacement potentials and the solution is obtained through an asymptotic analysis assuming a linear variation of elastic modulus with a constant density in Section 2. In Section 3, the solution for an identical exponential variation of elastic properties and density is obtained by employing the same procedure as used in Section 2. In Section 4, using the stress and displacement fields obtained in Sections 2 and 3, the characteristics of stress and displacement components around a propagating crack tip are examined for different crack speeds and nonhomogeneity.

2. Stress and displacement fields for a linear variation of elastic properties with a constant density

2.1. Formation for equilibrium equations

When the FGM has a linearly increasing shear modulus such as $\mu = \mu_0(1 + \varsigma X)$ under a constant density ρ and Poisson's ratio v, the relationship between stresses and strains can be written as

$$\begin{aligned} \sigma_X &= [a_{11}\varepsilon_X + a_{12}\varepsilon_Y](1 + \varsigma X) \\ \sigma_Y &= [a_{12}\varepsilon_X + a_{11}\varepsilon_Y](1 + \varsigma X) \\ \tau_{XY} &= \mu_0\gamma_{XY}(1 + \varsigma X) \end{aligned} \tag{1}$$

where X is the reference coordinate, σ_{ij} the inplane stress components, $a_{11} = \lambda_0 + 2\mu_0$ and $a_{12} = \lambda_0$, and λ_0 and μ_0 denoting Lame's constant and the shear modulus at $X = 0$, respectively. ς is the nonhomogeneity constant which has dimension $(\text{length})^{-1}$. It should be noted in this case that the longitudinal and shear wave speeds of the medium are variable.

If the deformation is plane strain, the displacements u and v which are derived from dilatational and shear wave potentials Φ and Ψ can be expressed by Eq. (2)

$$u = \frac{\partial \Phi}{\partial X} + \frac{\partial \Psi}{\partial Y}, \quad v = \frac{\partial \Phi}{\partial Y} - \frac{\partial \Psi}{\partial X} \tag{2}$$

The equilibrium in dynamic state is given by Eq. (3)

$$\frac{\partial \sigma_X}{\partial X}+\frac{\partial \tau_{XY}}{\partial Y}=\rho\frac{\partial^2 u}{\partial t^2},\quad \frac{\partial \tau_{XY}}{\partial X}+\frac{\partial \sigma_Y}{\partial Y}=\rho\frac{\partial^2 v}{\partial t^2} \tag{3}$$

Substituting Eq. (2) into Eq. (1), and substituting Eq. (1) into Eq. (3), the equations for the dynamic state can be obtained as

$$\frac{\partial}{\partial X}\left\{(1+\varsigma X)(k+2)\nabla^2\Phi-\frac{\rho}{\mu_0}\frac{\partial^2\Phi}{\partial t^2}\right\}+\frac{\partial}{\partial Y}\left\{(1+\varsigma X)\nabla^2\Psi-\frac{\rho}{\mu_0}\frac{\partial^2\Psi}{\partial t^2}\right\}-2\varsigma\left\{\frac{\partial^2\Phi}{\partial Y^2}-\frac{\partial^2\Psi}{\partial X\partial Y}\right\}=0 \tag{4a}$$

$$\frac{\partial}{\partial Y}\left\{(1+\varsigma X)(k+2)\nabla^2\Phi-\frac{\rho}{\mu_0}\frac{\partial^2\Phi}{\partial t^2}\right\}-\frac{\partial}{\partial X}\left\{(1+\varsigma X)\nabla^2\Psi-\frac{\rho}{\mu_0}\frac{\partial^2\Psi}{\partial t^2}\right\}+2\varsigma\left\{\frac{\partial^2\Psi}{\partial Y^2}+\frac{\partial^2\Phi}{\partial X\partial Y}\right\}=0 \tag{4b}$$

where $k=\lambda_0/\mu_0$, Eq. (4) can be satisfied when expressed as Eq. (5)

$$(1+\varsigma X)(k+2)\nabla^2\Phi-\frac{\rho}{\mu_0}\frac{\partial^2\Phi}{\partial t^2}+2\varsigma\frac{\partial\Psi}{\partial Y}=0 \tag{5a}$$

$$(1+\varsigma X)\nabla^2\Psi-\frac{\rho}{\mu_0}\frac{\partial^2\Psi}{\partial t^2}-2\varsigma\frac{\partial\Phi}{\partial Y}=0 \tag{5b}$$

For a propagating crack, the transformed crack tip coordinates are $x=X-ct$, $y=Y$. From this relation, we can write the equations of motion for steady state can be written as

$$\alpha_l^2\frac{\partial^2\Phi}{\partial x^2}+\frac{\partial^2\Phi}{\partial y^2}+\beta x\left(\frac{\partial^2\Phi}{\partial x^2}+\frac{\partial^2\Phi}{\partial y^2}\right)+\frac{2\beta}{k+2}\frac{\partial\Psi}{\partial y}=0 \tag{6a}$$

$$\alpha_s^2\frac{\partial^2\Psi}{\partial x^2}+\frac{\partial^2\Psi}{\partial y^2}+\beta x\left(\frac{\partial^2\Psi}{\partial x^2}+\frac{\partial^2\Psi}{\partial y^2}\right)-2\beta\frac{\partial\Phi}{\partial y}=0 \tag{6b}$$

where

$$\alpha_l=\sqrt{1-\left(\frac{c}{c_l}\right)^2},\quad \alpha_s=\sqrt{1-\left(\frac{c}{c_s}\right)^2},\quad c_s=\sqrt{\frac{\mu_c}{\rho}}$$

$$c_l=c_s\sqrt{\frac{2(1-\nu)}{1-2\nu}}\ \text{ for plane strain},\quad c_l=c_s\sqrt{\frac{2}{1-\nu}}\ \text{ for plane stress},$$

$$\mu_c=\mu_0(1+a\varsigma),\quad \beta(a,\varsigma)=\varsigma\frac{\mu_0}{\mu_c}=\frac{\varsigma}{1+a\varsigma}$$

The a is half the crack length in a center crack or the crack length of an edge crack. μ_c and μ_0 are shear modulus at the crack tip and $x=-a$, respectively. c, c_l and c_s are the crack propagation velocity, elastic dilatational wave velocity and elastic shear wave velocity at the crack tip. In this case, $\beta(a,\varsigma)$ is dependent on the crack length and the nonhomogeneity constant ς. It is very difficult to obtain analytical solutions for the elastodynamic differential equation (6). Thus, an asymptotic analysis similar to that employed by Freund (1990) is used to expand the stress field around the propagating crack. To obtain an asymptotic expansion of the fields around the crack tip, the crack tip coordinates are scaled to fill the entire field of

observation (Freund, 1990). This can be achieved by introducing new coordinates $\eta_1 = x/\varepsilon$, $\eta_2 = y/\varepsilon$ and ε is a small arbitrary positive number. For very small values of ε, the points very close to the crack tip are mapped into the range of observation in the η_1, η_2 plane. In the scale coordinates, Eq. (6) takes the form

$$\alpha_l^2 \frac{\partial^2 \Phi}{\partial \eta_1^2} + \frac{\partial^2 \Phi}{\partial \eta_2^2} + \varepsilon\beta\left[\eta_1\left(\frac{\partial^2 \Phi}{\partial \eta_1^2} + \frac{\partial^2 \Phi}{\partial \eta_2^2}\right) + \frac{2}{k+2}\frac{\partial \Psi}{\partial \eta_2}\right] = 0 \tag{7a}$$

$$\alpha_s^2 \frac{\partial^2 \Psi}{\partial \eta_1^2} + \frac{\partial^2 \Psi}{\partial \eta_2^2} + \varepsilon\beta\left[\eta_1\left(\frac{\partial^2 \Psi}{\partial \eta_1^2} + \frac{\partial^2 \Psi}{\partial \eta_2^2}\right) - 2\frac{\partial \Phi}{\partial \eta_2}\right] = 0 \tag{7b}$$

At this stage it is assumed that Φ and Ψ can be expanded by powers of ε as

$$\begin{aligned} \Phi(x,y) &= \Phi(\varepsilon\eta_1, \varepsilon\eta_2) = \sum_{n=1}^{\infty} \varepsilon^{n/2+1} \Phi_n(\eta_1, \eta_2) \\ \Psi(x,y) &= \Psi(\varepsilon\eta_1, \varepsilon\eta_2) = \sum_{n=1}^{\infty} \varepsilon^{n/2+1} \Psi_n(\eta_1, \eta_2) \end{aligned} \tag{8}$$

as $r = \sqrt{x^2 + y^2} \to 0$ and ε is a small arbitrary value. Substituting Eq. (8) into Eq. (7) and setting the partial differential equations associated with each power of ε to zero, the coupled differential equations for Φ_n and Ψ_n can be obtained.

$$\alpha_l^2 \frac{\partial^2 \Phi_n}{\partial \eta_1^2} + \frac{\partial^2 \Phi_n}{\partial \eta_2^2} = -\beta\eta_1\left(\frac{\partial^2 \Phi_{n-2}}{\partial \eta_1^2} + \frac{\partial^2 \Phi_{n-2}}{\partial \eta_2^2}\right) - \frac{2\beta}{k+2}\frac{\partial \Psi_{n-2}}{\partial \eta_2} \tag{9a}$$

$$\alpha_s^2 \frac{\partial^2 \Psi_n}{\partial \eta_1^2} + \frac{\partial^2 \Psi_n}{\partial \eta_2^2} = -\beta\eta_1\left(\frac{\partial^2 \Psi_{n-2}}{\partial \eta_1^2} + \frac{\partial^2 \Psi_{n-2}}{\partial \eta_2^2}\right) + 2\beta\frac{\partial \Phi_{n-2}}{\partial \eta_2} \tag{9b}$$

The Φ_n and Ψ_n have the complex functions $z_l(\eta_1, \mathrm{i}\alpha_l\eta_2)$ and $z_s(\eta_1, \mathrm{i}\alpha_s\eta_2)$, respectively, and $\Phi_n = \Psi_n = 0$ if $n < 0$. When the $\varsigma = 0$, the right side terms of equation become zero.

2.2. The stress and displacement fields for $n = 1, 2$

From Eq. (9), the differential equations for $n = 1$ and 2 are given in Eq. (10)

$$\alpha_l^2 \frac{\partial^2 \Phi_n}{\partial \eta_1^2} + \frac{\partial^2 \Phi_n}{\partial \eta_2^2} = 0, \quad \alpha_s^2 \frac{\partial^2 \Psi_n}{\partial \eta_1^2} + \frac{\partial^2 \Psi_n}{\partial \eta_2^2} = 0 \tag{10}$$

Eq. (10) is the Laplace equation and the same as that for a homogeneous material. The general solutions of Eq. (10) for fields Φ_n and Ψ_n can be assumed as

$$\begin{aligned} \Phi_n(\eta_1, \eta_2) &= -\mathrm{Re}\int \phi_n(z_l)\,\mathrm{d}z_l \\ \Psi_n(\eta_1, \eta_2) &= -\mathrm{Im}\int \psi_n(z_s)\,\mathrm{d}z_s \end{aligned} \tag{11}$$

Substituting the differentiation of Φ_n and Ψ_n in Eq. (11) into Eq. (2), the displacements in scaled plane can be obtained as $\varepsilon^{n/2}\{\phi_n(\eta_1, \eta_2), \psi_n(\eta_1\eta_2)\}$. Thus, the displacements u and v in the unscaled physical plane for $n = 1$ and 2 can be expressed as Eq. (12).

$$\begin{aligned} u &= -\mathrm{Re}\{\phi_n(z_l) + \alpha_s\psi_n(z_s)\} \\ v &= \mathrm{Im}\{\alpha_l\phi_n(z_l) + \psi_n(z_s)\} \end{aligned} \tag{12}$$

Substituting the differentiation of Eq. (12) into Eq. (1), the stress fields in the scaled plane can be obtained as $\varepsilon^{n/2-1}\mu\{\phi_n(\eta_1,\eta_2),\psi_n(\eta_1\eta_2)\}$. Thus the stress σ_{ij} in the unscaled physical plane for $n=1$ and 2 can be expressed as Eq. (13).

$$\begin{aligned}\sigma_x &= -\mu\mathrm{Re}\{(1+2\alpha_l^2-\alpha_s^2)\phi_n'(z_l)+2\alpha_s\psi_n'(z_s)\}\\ \sigma_y &= \mu\mathrm{Re}\{(1+\alpha_s^2)\phi_n'(z_l)+2\alpha_s\psi_n'(z_s)\}\\ \tau_{xy} &= \mu\mathrm{Im}\{2\alpha_l\phi_n'(z_l)+(1+\alpha_s^2)\psi_n'(z_s)\}\end{aligned} \tag{13}$$

The $\phi_n(z_l)$ and $\psi_n(z_l)$ can be written with a power series as

$$\phi_n(z_l)=\sum_{n=1}^{2}A_n z_l^{n/2},\quad \psi_n(z_s)=\sum_{n=1}^{2}B_n z_s^{n/2} \tag{14}$$

where A_n and B_n are complex constants and $z_l = x+\mathrm{i}\alpha_l y$ and $z_s = x+\mathrm{i}\alpha_s y$. Substituting Eq. (14) into Eq. (13), applying traction free boundary conditions on the crack surface to Eq. (13), the stresses for propagating crack in unscaled physical plane can be obtained as Eq. (15).

$$\sigma_{xn}=(1+\beta x)\sum_{n=1}^{2}\sigma_{xn}^0,\quad \sigma_{yn}=(1+\beta x)\sum_{n=1}^{2}\sigma_{yn}^0,\quad \tau_{xyn}=(1+\beta x)\sum_{n=1}^{2}\tau_{xyn}^0 \tag{15}$$

where

$$\begin{aligned}\sigma_{xn}^0 &= \frac{K_n^0 B_{\mathrm{I}}(c)}{\sqrt{2\pi}}n\left\{(1+2\alpha_l^2-\alpha_s^2)r_l^{\frac{n-2}{2}}\cos\left(\frac{n-2}{2}\right)\theta_l-2\alpha_s h(n)r_s^{\frac{n-2}{2}}\cos\left(\frac{n-2}{2}\right)\theta_s\right\}\\ &\quad+\frac{K_n^* B_{\mathrm{II}}(c)}{\sqrt{2\pi}}n\left\{(1+2\alpha_l^2-\alpha_s^2)r_l^{\frac{n-2}{2}}\sin\left(\frac{n-2}{2}\right)\theta_l-2\alpha_s h(\bar{n})r_s^{\frac{n-2}{2}}\sin\left(\frac{n-2}{2}\right)\theta_s\right\}\\ \sigma_{yn}^0 &= \frac{K_n^0 B_{\mathrm{I}}(c)}{\sqrt{2\pi}}n\left\{-(1+\alpha_s^2)r_l^{\frac{n-2}{2}}\cos\left(\frac{n-2}{2}\right)\theta_l+2\alpha_s h(n)r_s^{\frac{n-2}{2}}\cos\left(\frac{n-2}{2}\right)\theta_s\right\}\\ &\quad+\frac{K_n^* B_{\mathrm{II}}(c)}{\sqrt{2\pi}}n\left\{-(1+\alpha_s^2)r_l^{\frac{n-2}{2}}\sin\left(\frac{n-2}{2}\right)\theta_l+2\alpha_s h(\bar{n})r_s^{\frac{n-2}{2}}\sin\left(\frac{n-2}{2}\right)\theta_s\right\}\\ \tau_{xyn}^0 &= \frac{K_n^0 B_{\mathrm{I}}(c)}{\sqrt{2\pi}}n\left\{-2\alpha_l r_l^{\frac{n-2}{2}}\sin\left(\frac{n-2}{2}\right)\theta_l+(1+\alpha_s^2)h(n)r_s^{\frac{n-2}{2}}\sin\left(\frac{n-2}{2}\right)\theta_s\right\}\\ &\quad+\frac{K_n^* B_{\mathrm{II}}(c)}{\sqrt{2\pi}}n\left\{2\alpha_l r_l^{\frac{n-2}{2}}\cos\left(\frac{n-2}{2}\right)\theta_l-(1+\alpha_s^2)h(\bar{n})r_s^{\frac{n-2}{2}}\cos\left(\frac{n-2}{2}\right)\theta_s\right\}\end{aligned}$$

The displacement for propagating crack in an unscaled physical plane can be obtained as Eq. (16).

$$u_n=\frac{1}{(1+\zeta a)}\sum_{n=1}^{2}u_n^0,\quad v_n=\frac{1}{(1+\zeta a)}\sum_{n=1}^{2}v_n^0 \tag{16}$$

where

$$u_n^0=\frac{K_n^0 B_{\mathrm{I}}(c)}{\mu_0}\sqrt{\frac{2}{\pi}}\left\{r_l^{\frac{n}{2}}\cos\left(\frac{n}{2}\right)\theta_l-\alpha_s h(n)r_s^{\frac{n}{2}}\cos\left(\frac{n}{2}\right)\theta_s\right\}+\frac{K_n^* B_{\mathrm{II}}(c)}{\mu_0}\sqrt{\frac{2}{\pi}}\left\{r_l^{\frac{n}{2}}\sin\left(\frac{n}{2}\right)\theta_l-\alpha_s h(\bar{n})r_s^{\frac{n}{2}}\sin\left(\frac{n}{2}\right)\theta_s\right\}$$

$$v_n^0 = \frac{K_n^0 B_{\mathrm{I}}(c)}{\mu_0}\sqrt{\frac{2}{\pi}}\left\{-\alpha_{\mathrm{l}} r_{\mathrm{l}}^{\frac{n}{2}}\sin\left(\frac{n}{2}\right)\theta_{\mathrm{l}} + h(n) r_{\mathrm{s}}^{\frac{n}{2}}\sin\left(\frac{n}{2}\right)\theta_{\mathrm{s}}\right\} + \frac{K_n^* B_{\mathrm{II}}(c)}{\mu_0}\sqrt{\frac{2}{\pi}}\left\{\alpha_{\mathrm{l}} r_{\mathrm{l}}^{\frac{n}{2}}\cos\left(\frac{n}{2}\right)\theta_{\mathrm{l}} - h(\bar{n}) r_{\mathrm{s}}^{\frac{n}{2}}\cos\left(\frac{n}{2}\right)\theta_{\mathrm{s}}\right\}$$

$$r_j = \sqrt{x^2 + (\alpha_j y)^2}, \quad \theta_j = \tan^{-1}(\alpha_j y/x), \quad j = \mathrm{l}, \mathrm{s}$$

$$h(n) = \frac{2\alpha_{\mathrm{l}}}{1+\alpha_{\mathrm{s}}^2}(n = \text{odd}), \quad \frac{1+\alpha_{\mathrm{s}}^2}{2\alpha_{\mathrm{s}}}(n = \text{even}), \quad \bar{n} = n+1$$

$$B_{\mathrm{I}}(c) = \frac{1+\alpha_{\mathrm{s}}^2}{4\alpha_{\mathrm{l}}\alpha_{\mathrm{s}} - (1+\alpha_{\mathrm{s}}^2)^2}, \quad B_{\mathrm{II}}(c) = \frac{2\alpha_{\mathrm{s}}}{4\alpha_{\mathrm{l}}\alpha_{\mathrm{s}} - (1+\alpha_{\mathrm{s}}^2)^2}$$

K_{I}^0 and K_{II}^0 for $n = 1$ are the stress intensity factors K_{I} and K_{II}, respectively. When $n = 1$ and 2, the differential equations in Eq. (10) are the same as those for a homogeneous material (Freund, 1990) but their stress and displacement fields are influenced by the nonhomogeneity constant ς.

2.3. Stress and displacement fields for $n = 3$

For $n \geqslant 3$ in Eq. (9), the Φ_n and Ψ_n become nonhomogeneous fields, and only $n = 3$ is considered to generate the fields in this study. To solve Eq. (9), the relation between $\Phi_1(z_{\mathrm{l}})$ and $\Psi_1(z_{\mathrm{s}})$ must be known. If the relation between $\Phi_1(z_{\mathrm{l}})$ and $\Psi_1(z_{\mathrm{s}})$ does not apply to Eq. (9), the dilatational and rotational terms in the equations of motion remain coupled. This causes the stress fields to be infinite when the crack velocity approaches zero. Considering Eq. (10), the relation between $\Phi_1(z_{\mathrm{l}})$ and $\Psi_1(z_s)$ can be obtained when the ς terms in Eq. (4) are zero. Thus, the relations can be expressed as (see Appendix A).

$$\frac{\partial}{\partial\eta_2}\Psi_1(z_{\mathrm{s}}) = -\frac{A(\alpha_{\mathrm{l}})}{B(\alpha_{\mathrm{s}})}\frac{\partial}{\partial\eta_1}\Phi_1(z_{\mathrm{l}}) = -(k+2)\frac{\partial}{\partial\eta_1}\Phi_1(z_{\mathrm{l}}) \tag{17a}$$

$$\frac{1}{k+2}\frac{\partial}{\partial\eta_1}\Psi_1(z_{\mathrm{s}}) = \frac{\partial}{\partial\eta_2}\Phi_1(z_{\mathrm{l}}) \tag{17b}$$

where

$$A(\alpha_{\mathrm{l}}) = (k+2)\left[(1-\alpha_{\mathrm{l}}^2) - \frac{\rho c^2}{\mu_0(k+2)}\right], \quad B(\alpha_{\mathrm{s}}) = (1-\alpha_{\mathrm{s}}^2) - \frac{\rho c^2}{\mu_0}$$

Substituting Eq. (17) into Eq. (9), Eq. (9) becomes as

$$\alpha_{\mathrm{l}}^2\frac{\partial^2\Phi_3}{\partial\eta_1^2} + \frac{\partial^2\Phi_3}{\partial\eta_2^2} = -\beta\eta_1\left(\frac{\partial^2\Phi_1}{\partial\eta_1^2} + \frac{\partial^2\Phi_1}{\partial\eta_2^2}\right) + 2\beta\frac{\partial\Phi_1}{\partial\eta_1} \tag{18a}$$

$$\alpha_{\mathrm{s}}^2\frac{\partial^2\Psi_3}{\partial\eta_1^2} + \frac{\partial^2\Psi_3}{\partial\eta_2^2} = -\beta\eta_1\left(\frac{\partial^2\Psi_1}{\partial\eta_1^2} + \frac{\partial^2\Psi_1}{\partial\eta_2^2}\right) + \frac{2\beta}{k+2}\frac{\partial\Psi_1}{\partial\eta_1} \tag{18b}$$

Let the right side terms $\Phi_1(z_{\mathrm{l}})$ and $\Psi_1(z_{\mathrm{s}})$ in Eq. (18) put $-\mathrm{Re}\int\Phi_1(z_{\mathrm{l}})\,\mathrm{d}z_{\mathrm{l}}$, $-\mathrm{Im}\int\Psi_1(z_{\mathrm{s}})\,dz_{\mathrm{s}}$, respectively, then the solutions for $\Phi_3(z_{\mathrm{l}})$ and $\Psi_3(z_{\mathrm{s}})$ can be obtained as

$$\Phi_3(\eta_1,\eta_2)=\mathrm{Re}\left\{-\int\phi_3(z_1)\,\mathrm{d}z_1+\beta\left[\frac{1-\alpha_1^2}{\alpha_1^2}\eta_1 r_1^2 a_j\phi_1'(z_1)-\frac{1}{3\alpha_1^2}r_1^2\phi_1(z_1)\right]\right\} \tag{19a}$$

$$\Psi_3(\eta_1,\eta_2)=\mathrm{Im}\left\{-\int\psi_3(z_s)\,\mathrm{d}z_s+\beta\left[\frac{1-\alpha_s^2}{\alpha_s^2}\eta_1 r_s^2 a_j\psi_1'(z_s)-\frac{1}{3(k+2)\alpha_s^2}r_s^2\psi_1(z_s)\right]\right\} \tag{19b}$$

where a_j is a coefficient of trigonometric function, and

$$a_j=\begin{cases}\frac{1}{4}:\left[a_j\cos\frac{3}{2}\theta_j,a_j\sin\frac{3}{2}\theta_j\right]\\ \frac{1}{6}:\left[a_j\cos\frac{1}{2}\theta_j,a_j\sin\frac{1}{2}\theta\right]\end{cases}$$

The first term on the right hand side in Eq. (19) corresponds to that for a homogeneous material and the additional term is the result of the nonhomogeneity of the material. The nonhomogeneous K displacement field obtained from Eq. (19), $u_{\mathrm{non}}(\beta,K)$ can be applied in $r\to 0$. However the displacement components obtained from the last terms in Eq. (19) approach very large values except when $r=0$ when the crack propagation velocity approaches zero. Such a behavior is not consistent with the physical meaning of $r>0$. Thus, the last terms can not be applied in the case where $r>0$. Substituting Eq. (19) into Eq. (2) and applying the traction free boundary condition to the crack surface, the components of displacement in the unscaled plane can be expressed as

$$\begin{aligned}u_3=\frac{1}{(1+\zeta a)}\Bigg\{&u_3^0-\beta\frac{K_{\mathrm{I}}B_{\mathrm{I}}(c)}{\mu_0\sqrt{2\pi}}\left[r_1^{3/2}\frac{(1-\alpha_1^2)}{\alpha_1^2}F(\theta_1)+r_s^{3/2}h_1\frac{(1-\alpha_s^2)}{\alpha_s}G(\theta_s)\right]\\&-\beta\frac{K_{\mathrm{II}}B_{\mathrm{II}}(c)}{\mu_0\sqrt{2\pi}}\left[r_1^{3/2}\frac{(1-\alpha_1^2)}{\alpha_1^2}H(\theta_1)+r_s^{3/2}\bar{h}_1\frac{(1-\alpha_s^2)}{\alpha_s}\mathrm{I}(\theta_s)\right]\Bigg\}\end{aligned} \tag{20}$$

$$\begin{aligned}v_3=\frac{1}{(1+\zeta a)}\Bigg\{&v_3^0-\beta\frac{K_{\mathrm{I}}B_{\mathrm{I}}(c)}{\mu_0\sqrt{2\pi}}\left[r_1^{3/2}\frac{(1-\alpha_1^2)}{\alpha_1}I(\theta_1)+r_s^{3/2}h_1\frac{(1-\alpha_s^2)}{\alpha_s^2}H(\theta_s)\right]\\&+\beta\frac{K_{\mathrm{II}}B_{\mathrm{II}}(c)}{\mu_0\sqrt{2\pi}}\left[r_1^{3/2}\frac{(1-\alpha_1^2)}{\alpha_1}G(\theta_1)+r_s^{3/2}\bar{h}_1\frac{(1-\alpha_s^2)}{\alpha_s^2}F(\theta_s)\right]\Bigg\}\end{aligned} \tag{21}$$

where

$$F(\theta_j)=\frac{1}{16}\cos\frac{5}{2}\theta_j+\frac{1}{12}\cos\frac{3\theta_j}{2}+\frac{3}{8}\cos\frac{\theta_j}{2},\quad G(\theta_j)=-\frac{1}{16}\cos\frac{5}{2}\theta_j+\frac{1}{12}\cos\frac{3\theta_j}{2}+\frac{1}{8}\cos\frac{\theta_j}{2}$$

$$H(\theta_j)=-\frac{1}{16}\sin\frac{5}{2}\theta_j+\frac{1}{12}\sin\frac{3\theta_j}{2}-\frac{3}{8}\sin\frac{\theta_j}{2}$$

$$I(\theta_j)=\frac{1}{16}\sin\frac{5}{2}\theta_j+\frac{1}{12}\sin\frac{3\theta_j}{2}-\frac{1}{8}\sin\frac{\theta_j}{2},\quad j=1,s$$

Substituting the differentiations of Eqs. (20) and (21) into Eq. (1), the stresses for a propagating crack in the unscaled plane can be obtained as

$$\sigma_{x3} = (1+\beta x)\left\{\sigma^0_{x3} + \beta\frac{K_{\mathrm{I}}B_{\mathrm{I}}(c)}{\sqrt{2\pi}}r_{\mathrm{l}}^{1/2}\left[(1+2\alpha_{\mathrm{l}}^2-\alpha_{\mathrm{s}}^2)A_1C_1(\theta_{\mathrm{l}}) - \frac{(1-\alpha_{\mathrm{s}}^2)}{(1-\alpha_{\mathrm{l}}^2)}\frac{A_1}{2}C_2(\theta_{\mathrm{l}})\right]\right.$$
$$+\beta\frac{K_{\mathrm{I}}B_{\mathrm{I}}(c)}{\sqrt{2\pi}}r_{\mathrm{s}}^{1/2}\left[-2\alpha_{\mathrm{s}}B_1h_1\left(\frac{1}{4}\cos\frac{1}{2}\theta_{\mathrm{s}} - \frac{1}{16}\cos\frac{3\theta_{\mathrm{s}}}{2} + \frac{1}{32}\cos\frac{7}{2}\theta_{\mathrm{s}}\right)\right]$$
$$+\beta\frac{K_{\mathrm{II}}B_{\mathrm{II}}(c)}{\sqrt{2\pi}}r_{\mathrm{l}}^{1/2}\left[-(1+2\alpha_{\mathrm{l}}^2-\alpha_{\mathrm{s}}^2)A_1S_1(\theta_{\mathrm{l}}) + \frac{(1-\alpha_{\mathrm{s}}^2)}{(1-\alpha_{\mathrm{l}}^2)}\frac{A_1}{2}S_2(\theta_{\mathrm{l}})\right]$$
$$\left.+\beta\frac{K_{\mathrm{II}}B_{\mathrm{II}}(c)}{\sqrt{2\pi}}r_{\mathrm{s}}^{1/2}\left[2\alpha_{\mathrm{s}}B_1\bar{h}_1\left(-\frac{1}{4}\sin\frac{1}{2}\theta_{\mathrm{s}} - \frac{1}{16}\sin\frac{3\theta_{\mathrm{s}}}{2} + \frac{1}{32}\sin\frac{7}{2}\theta_{\mathrm{s}}\right)\right]\right\} \tag{22}$$

$$\sigma_{y3} = (1+\beta x)\left\{\sigma^0_{y3} + \beta\frac{K_{\mathrm{I}}B_{\mathrm{I}}(c)}{\sqrt{2\pi}}r_{\mathrm{l}}^{1/2}\left[-(1+\alpha_{\mathrm{s}}^2)A_1C_1(\theta_{\mathrm{l}}) + \frac{(1+\alpha_{\mathrm{s}}^2-2\alpha_{\mathrm{l}}^2)}{(1-\alpha_{\mathrm{l}}^2)}\frac{A_1}{2}C_2(\theta_{\mathrm{l}})\right]\right.$$
$$+\beta\frac{K_{\mathrm{I}}B_{\mathrm{I}}(c)}{\sqrt{2\pi}}r_{\mathrm{s}}^{1/2}\left[2\alpha_{\mathrm{s}}B_1h_1\left(\frac{1}{4}\cos\frac{1}{2}\theta_{\mathrm{s}} - \frac{1}{16}\cos\frac{3\theta_{\mathrm{s}}}{2} + \frac{1}{32}\cos\frac{7}{2}\theta_{\mathrm{s}}\right)\right]$$
$$+\beta\frac{K_{\mathrm{II}}B_{\mathrm{II}}(c)}{\sqrt{2\pi}}r_{\mathrm{l}}^{1/2}\left[(1+\alpha_{\mathrm{s}}^2)A_1S_1(\theta_{\mathrm{l}}) - \frac{(1+\alpha_{\mathrm{s}}^2-2\alpha_{\mathrm{l}}^2)}{(1-\alpha_{\mathrm{l}}^2)}\frac{A_1}{2}S_2(\theta_{\mathrm{l}})\right]$$
$$\left.+\beta\frac{K_{\mathrm{II}}B_{\mathrm{II}}(c)}{\sqrt{2\pi}}r_{\mathrm{s}}^{1/2}\left[2\alpha_{\mathrm{s}}B_1\bar{h}_1\left(\frac{1}{4}\sin\frac{1}{2}\theta_{\mathrm{s}} + \frac{1}{16}\sin\frac{3\theta_{\mathrm{s}}}{2} - \frac{1}{32}\sin\frac{7}{2}\theta_{\mathrm{s}}\right)\right]\right\} \tag{23}$$

$$\tau_{xy3} = (1+\beta x)\left\{\tau^0_{xy3} + \beta\frac{K_{\mathrm{I}}B_{\mathrm{I}}(c)}{\sqrt{2\pi}}r_{\mathrm{l}}^{1/2}\left[-2\alpha_{\mathrm{l}}A_1\left(\frac{1}{4}\sin\frac{1}{2}\theta_{\mathrm{l}} + \frac{1}{16}\sin\frac{3\theta_{\mathrm{l}}}{2} - \frac{1}{32}\sin\frac{7}{2}\theta_{\mathrm{l}}\right)\right]\right.$$
$$+\beta\frac{K_{\mathrm{I}}B_{\mathrm{I}}(c)}{\sqrt{2\pi}}r_{\mathrm{s}}^{1/2}h_1B_1\left[-(1+\alpha_{\mathrm{s}}^2)S_1(\theta_{\mathrm{s}}) + \frac{1}{2}S_2(\theta_{\mathrm{s}})\right]$$
$$+\beta\frac{K_{\mathrm{II}}B_{\mathrm{II}}(c)}{\sqrt{2\pi}}r_{l}^{1/2}\left[-2\alpha_lA_1\left(-\frac{1}{4}\cos\frac{1}{2}\theta_l + \frac{1}{16}\cos\frac{3\theta_l}{2} - \frac{1}{32}\cos\frac{7}{2}\theta_l\right)\right]$$
$$\left.+\beta\frac{K_{\mathrm{II}}B_{\mathrm{II}}(c)}{\sqrt{2\pi}}r_{\mathrm{s}}^{1/2}\bar{h}_1B_1\left[-(1+\alpha_{\mathrm{s}}^2)C_1(\theta_{\mathrm{s}}) + \frac{1}{2}C_2(\theta_{\mathrm{s}})\right]\right\} \tag{24}$$

where

$$A_1 = \frac{1-\alpha_{\mathrm{l}}^2}{\alpha_{\mathrm{l}}^2}, \quad B_1 = \frac{1-\alpha_{\mathrm{s}}^2}{\alpha_{\mathrm{s}}^2}$$

$$C_1(\theta_j) = \frac{3}{16}\cos\frac{3}{2}\theta_j + \frac{1}{32}\cos\frac{7}{2}\theta_j, \quad C_2(\theta_j) = \cos\frac{1}{2}\theta_j + \cos\frac{3}{2}\theta_j$$

$$S_1(\theta_j) = \frac{3}{16}\sin\frac{3}{2}\theta_j + \frac{1}{32}\sin\frac{7}{2}\theta_j, \quad S_2(\theta_j) = \sin\frac{3}{2}\theta_j - \sin\frac{1}{2}\theta_j$$

$$h_1 = -\frac{14A_1\alpha_{\mathrm{l}}}{[32-7(1+\alpha_{\mathrm{s}}^2)]B_1}, \quad \bar{h}_1 = \frac{A_1\{(1+\alpha_{\mathrm{s}}^2)[7(1-\alpha_{\mathrm{l}}^2)-32]+64\alpha_{\mathrm{l}}^2\}}{[14\alpha_{\mathrm{s}}(1-\alpha_{\mathrm{l}}^2)]B_1}$$

Finally, the fields for FGM, σ_{ij} and u_j are given in Eq. (25)

$$\sigma_{ij} = \sum_{n=1}^{3}\sigma_{ijn}, \quad u_j = \sum_{n=1}^{3}u_{jn} \tag{25}$$

The stress fields in Eq. (25) satisfy the traction free condition on the crack surface ($\theta = \pm\pi$). When the nonhomogeneity parameter $\varsigma = 0$, the equations reduce to the fields for an isotropic homogeneous material. It can be observed from the stress and displacement fields (Eqs. (20)–(24)) that, due to nonhomogeneity, the higher order terms ($n = 3$ and above) involve additional expressions containing the stress intensity factor. However, these additional expressions scaled by the nonhomogeneity parameter, β (for example see Eqs. (20)–(24)) become insignificant compared to the singular term of the expansion at the crack tip. Thus, very close to the crack tip, the stress and displacement fields can be adequately represented by the solution for homogeneous materials. However, the stress and displacement field that is remote from the crack tip must be expressed by Eq. (25) which contains nonhomogeneity specific expressions. Generally, in order to obtain the fracture parameters for a homogeneous material from experimental data obtained through optical techniques such as photoelasticity or coherent gradient sensing (CGS) the use of the first few terms of the stress fields is sufficient. The coefficient of term $n = 1(r^{-1/2}f_{ij})$ is proportional to the stress intensity factor and that of the term $n = 2(r^0 f_{ij})$ is the uniform stress σ_{ox} in the direction of the crack. In FGMs, it is necessary to use at least three terms of the fields to explicitly account for the nonhomogeneity effects when extracting fracture parameters from experimental data.

3. Stress and displacement fields for an exponential variation of elastic properties and density

The elastic constants μ and ρ of FGM are assumed to vary in an exponential manner as given by Eq. (26), where as the Poisson's ratio v is assumed to be constant.

$$\mu = \mu_0 \exp(\zeta X), \quad \rho = \rho_0 \exp(\zeta X) \tag{26}$$

μ_0 and ρ_0 are shear modulus at $X = 0$, respectively, and ς is the nonhomogeneity constant. By employing the same procedure used in Section 2.1, the equilibrium equation for exponential variation of elastic properties can be obtained as

$$\frac{\partial}{\partial X}\left\{(k+2)\nabla^2\Phi - \frac{\rho_0}{\mu_0}\frac{\partial^2\Phi}{\partial t^2}\right\} + \frac{\partial}{\partial Y}\left\{\nabla^2\Psi - \frac{\rho_0}{\mu_0}\frac{\partial^2\Psi}{\partial t^2}\right\} + \zeta\left\{k\nabla^2\Phi + 2\frac{\partial^2\Phi}{\partial X^2} + 2\frac{\partial^2\Psi}{\partial X\partial Y}\right\} = 0 \tag{27a}$$

$$\frac{\partial}{\partial \mathrm{Y}}\left\{(k+2)\nabla^2\Phi - \frac{\rho_0}{\mu_0}\frac{\partial^2\Phi}{\partial t^2}\right\} - \frac{\partial}{\partial \mathrm{X}}\left\{\nabla^2\Psi - \frac{\rho_0}{\mu_0}\frac{\partial^2\Psi}{\partial t^2}\right\} + \zeta\left\{2\frac{\partial^2\Phi}{\partial \mathrm{X}\partial \mathrm{Y}} + \frac{\partial^2\Psi}{\partial \mathrm{Y}^2} - \frac{\partial^2\Psi}{\partial \mathrm{X}^2}\right\} = 0 \tag{27b}$$

where $k = \lambda_0/\mu_0$. For a propagating crack the transformed crack tip coordinates are $x = X - ct$, $y = Y$. Thus, Eq. (27) can be expressed as

$$\alpha_l^2\frac{\partial^2\Phi}{\partial x^2} + \frac{\partial^2\Phi}{\partial y^2} + \zeta\frac{\partial\Phi}{\partial x} + \frac{\zeta}{k+2}\frac{\partial\Psi}{\partial y} = 0 \tag{28a}$$

$$\alpha_s^2\frac{\partial^2\Psi}{\partial x^2} + \frac{\partial^2\Psi}{\partial y^2} + \zeta\frac{\partial\Psi}{\partial x} + \zeta k\frac{\partial\Phi}{\partial y} = 0 \tag{28b}$$

It should be noted here that, Eq. (28), unlike Eq. (6) for the linear variation of elastic properties, have coefficients which are all constants. Hence, for crack speeds that are less than the shear wave speed of the material, the partial differential equation is elliptic over the entire domain. However, the form of the equation is still different from the classical wave equation. The same procedure used in the previous section is used to obtain the asymptotic expansion of the displacement and stress fields. For n equal to 1 and 2, the partial differential equations and their solutions are the same as those in the case of linear variation and hence, the crack tip stress and displacement fields can be expressed as

$$\sigma_{xn} = \mathrm{e}^{\zeta x}\sum_{n=1}^{2}\sigma_{xn}^{0}, \quad \sigma_{yn} = \mathrm{e}^{\zeta x}\sum_{n=1}^{2}\sigma_{yn}^{0}, \quad \tau_{xyn} = \mathrm{e}^{\zeta x}\sum_{n=1}^{2}\tau_{xyn}^{0} \tag{29}$$

The displacement for propagating crack in unscaled physical plane can be obtained as Eq. (30).

$$u_n = \mathrm{e}^{-\varsigma a}\sum_{n=1}^{2}u_n^{0}, \quad v_n = \mathrm{e}^{-\zeta a}\sum_{n=1}^{2}v_n^{0} \tag{30}$$

The form of the partial differential equation for n greater than 2 is somewhat different from Eq. (9) and is given as

$$\alpha_1^2\frac{\partial^2\Phi_n}{\partial\eta_1^2} + \frac{\partial^2\Phi_n}{\partial\eta_2^2} = -\zeta\left[\frac{\partial\Phi_{n-2}}{\partial\eta_1} + \frac{1}{k+2}\frac{\partial\Psi_{n-2}}{\partial\eta_2}\right] \tag{31a}$$

$$\alpha_{\mathrm{s}}^2\frac{\partial^2\Psi_n}{\partial\eta_1^2} + \frac{\partial^2\Psi_n}{\partial\eta_2^2} = -\zeta\left[\frac{\partial\Psi_{n-2}}{\partial\eta_1} + k\frac{\partial\Phi_{n-2}}{\partial\eta_2}\right] \tag{31b}$$

Applying the relation between $\Phi_1(z_1)$ and $\Psi_1(z_{\mathrm{s}})$ in Eq. (17) to Eq. (31), Eq. (31) becomes as

$$\alpha_1^2\frac{\partial^2\Phi_3}{\partial\eta_1^2} + \frac{\partial^2\Phi_3}{\partial\eta_2^2} = 0 \tag{32}$$

$$\alpha_s^2\frac{\partial^2\Psi_3}{\partial\eta_1^2} + \frac{\partial^2\Psi_3}{\partial\eta_2^2} = -\zeta\left[(1-d_{\mathrm{s}})\frac{\partial\Psi_1}{\partial\eta_1}\right] \tag{33}$$

where

$$d_{\mathrm{s}} = \frac{-k}{k+2} = \frac{1+\alpha_s^2-2\alpha_1^2}{1-\alpha_{\mathrm{s}}^2}$$

Let the right side term $\Psi_1(z_1)$ in Eq. (33) put $-\mathrm{Im}\int\psi_1(z_{\mathrm{s}})\,dz_s$, then the $\Phi_3(z_1)$ and $\Psi_3(z_s)$ can be obtained as

$$\begin{aligned}\Phi_3(\eta_1,\eta_2) &= \mathrm{Re}\left\{-\int\phi_3(z_1)\,\mathrm{d}z_1\right\}\\ \Psi_3(\eta_1,\eta_2) &= \mathrm{Im}\left\{-\int\psi_3(z_{\mathrm{s}})\,\mathrm{d}z_{\mathrm{s}} + \zeta\frac{1-d_{\mathrm{s}}}{6\alpha_{\mathrm{s}}^2}r_{\mathrm{s}}^2\psi_1(z_{\mathrm{s}})\right\}\end{aligned} \tag{34}$$

Substituting Eq. (34) into Eq. (2), the components of displacement in the unscaled plane can be expressed as

$$\begin{aligned}u_3 = \exp(-\zeta a)\Bigg\{&u_3^0 - \zeta\frac{K_{\mathrm{I}}B_{\mathrm{I}}(c)}{\mu_0\sqrt{2\pi}}\left[r_{\mathrm{s}}^{3/2}\frac{1}{\alpha_{\mathrm{s}}}h(1-d_{\mathrm{s}})\left(\frac{1}{3}\cos\frac{3\theta_{\mathrm{s}}}{2} - \frac{1}{2}\cos\frac{\theta_{\mathrm{s}}}{2}\right)\right]\\ &- \zeta\frac{K_{\mathrm{II}}B_{\mathrm{II}}(c)}{\mu_0\sqrt{2\pi}}\left[r_{\mathrm{s}}^{3/2}\frac{1}{\alpha_{\mathrm{s}}}\bar{h}(1-d_{\mathrm{s}})\left(\frac{1}{3}\sin\frac{3\theta_{\mathrm{s}}}{2} + \frac{1}{2}\sin\frac{\theta_{\mathrm{s}}}{2}\right)\right]\Bigg\}\end{aligned} \tag{35}$$

$$\begin{aligned}v_3 = \exp(-\zeta a)\Bigg\{&v_3^0 - \zeta\frac{K_{\mathrm{I}}B_{\mathrm{I}}(c)}{\mu_0\sqrt{2\pi}}\left[r_{\mathrm{s}}^{3/2}\frac{1}{\alpha_{\mathrm{s}}^2}h(1-d_{\mathrm{s}})\left(\frac{1}{3}\sin\frac{3\theta_{\mathrm{s}}}{2} - \frac{1}{2}\sin\frac{\theta_{\mathrm{s}}}{2}\right)\right]\\ &+ \zeta\frac{K_{\mathrm{II}}B_{\mathrm{II}}(c)}{\mu_0\sqrt{2\pi}}\left[r_{\mathrm{s}}^{3/2}\frac{1}{\alpha_{\mathrm{s}}^2}\bar{h}(1-d_{\mathrm{s}})\left(\frac{1}{3}\cos\frac{3\theta_{\mathrm{s}}}{2} + \frac{1}{2}\cos\frac{\theta_{\mathrm{s}}}{2}\right)\right]\Bigg\}\end{aligned} \tag{36}$$

Substituting the differentiations of Eqs. (35) and (36) into Eq. (1), the stresses for a propagating crack in unscaled plane can be obtained as

$$\sigma_{x3} = \exp(\zeta x)\left\{\sigma^0_{x3} + \zeta\frac{K_{\mathrm{I}}B_{\mathrm{I}}(c)}{\sqrt{2\pi}}r_{\mathrm{s}}^{1/2}\alpha_{\mathrm{s}}\left[\frac{Bh}{2}\cos\frac{3\theta_{\mathrm{s}}}{2}\right] + \zeta\frac{K_{\mathrm{II}}B_{\mathrm{II}}(c)}{\sqrt{2\pi}}r_{s}^{1/2}\alpha_{\mathrm{s}}\left[\frac{-B}{2}\bar{h}\sin\frac{3\theta_{\mathrm{s}}}{2}\right]\right\} \tag{37}$$

$$\sigma_{y3} = \exp(\zeta x)\left\{\sigma^0_{y3} + \zeta\frac{K_{\mathrm{I}}B_{\mathrm{I}}(c)}{\sqrt{2\pi}}r_{\mathrm{s}}^{1/2}\alpha_{\mathrm{s}}\left[-\frac{B}{2}h\cos\frac{3\theta_{\mathrm{s}}}{2}\right] + \zeta\frac{K_{\mathrm{II}}B_{\mathrm{II}}(c)}{\sqrt{2\pi}}r_{\mathrm{s}}^{1/2}\alpha_{\mathrm{s}}\left[\frac{B}{2}\bar{h}\sin\frac{3\theta_{\mathrm{s}}}{2}\right]\right\} \tag{38}$$

$$\begin{aligned}\tau_{xy3} = \exp(\zeta x)\Bigg\{&\tau^0_{xy3} + \zeta\frac{K_{\mathrm{I}}B_{\mathrm{I}}(c)}{\sqrt{2\pi}}r_{\mathrm{s}}^{1/2}Bh\left[-(1-\alpha_{\mathrm{s}}^2)\sin\frac{\theta_{\mathrm{s}}}{2} + \frac{1+\alpha_{\mathrm{s}}^2}{4}\sin\frac{3\theta_{\mathrm{s}}}{2}\right]\\ &+ \zeta\frac{K_{\mathrm{II}}B_{\mathrm{II}}(c)}{\sqrt{2\pi}}r_{\mathrm{s}}^{1/2}B\bar{h}\left[(1-\alpha_{\mathrm{s}}^2)\cos\frac{\theta_{\mathrm{s}}}{2} + \frac{1+\alpha_{\mathrm{s}}^2}{4}\cos\frac{3\theta_{\mathrm{s}}}{2}\right]\Bigg\}\end{aligned} \tag{39}$$

where

$$B = \frac{1-d_{\mathrm{s}}}{\alpha_{\mathrm{s}}^2}$$

Even if the stresses for $n = 3$ are expressed as the above equations, considering the traction free conditions on a crack surface ($\theta = \pm\pi$), h and $\bar{h}$ must be zero. Thus, the fields σ_{ij} and u_j for an exponential variation in elastic properties and density are can be expressed as Eq. (40).

$$\sigma_{ij} = \exp(\zeta x)\sum_{n=1}^{\infty}\sigma^0_{ijn}, \quad u_j = \exp(-\zeta a)\sum_{n=1}^{\infty}u^0_{jn} \tag{40}$$

The stress fields around the crack tip (x is small) in Eq. (40) can be expressed as

$$\sigma_{ij} \cong \sigma^0_{ij1} + \sigma^0_{ij2}(\sigma_{0x}) + \zeta x[\sigma^0_{ij1} + \sigma_{0x}] + \cdots \tag{41}$$

As is known from Eq. (41), higher order terms of stresses at the crack tip in the form of an asymptotic expansion show the coefficients of $r^{-1/2}$ and r^0 to also be identical to those present in the asymptotic the behavior of a formulation of homogeneous crack tip. Only terms of the order $r^{1/2}$ and beyond would be influenced by such a gradient, which would have coefficients different from those of homogeneous materials. However, higher terms of displacements at the crack tip as an asymptotic expansion would be influenced not by ςx but by ςa.

4. Characteristics of a propagating crack in an FGM

4.1. Effect of nonhomogeneity on stress fields

In order to investigate the effects of nonhomogeneity on stress components close to the crack tip, Eq. (41) for the exponential variation of elastic properties is used. To analyze the isochromatic fringe patterns that are remote from the crack tip, Eqs. (25) and (41) are used. In addition, all the coefficients other than those proportional to the stress intensity factor are assumed to be zero. The stress components (see Fig. 1) were evaluated as a function of the angular position (θ) at three different radial locations (r) for a near stationary crack and for a crack propagating at $M = 0.7$, where M is c/c_{s}. The mechanical properties of the particulate FGM developed by Parameswaran and Shukla (2000), as shown in Table 1, were used. The variation of the elastic modulus for this FGM is shown in Fig. 2, along with the exponential fit. Figs. 3–5 show the angular variation of the normalized stress components for a mode I crack and Figs. 6–8 show the

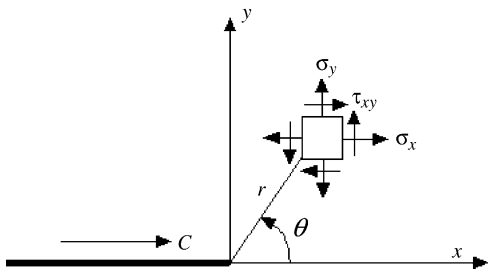

Fig. 1. Stress components in the vicinity of the crack tip.

Table 1
Mechanical properties for a polyester FGM

Nonhomogeneous shear modulus, $\mu(X)$	$\mu(X) = 1.316e^{\varsigma X}$ (GPa)
FGM constant, ς	$\varsigma = 1.19/\text{m}$
Poisson's ratio, v	$v = 0.33$
Density at $X = 0$, ρ_0	$\rho_0 = 1200$ (kg/m^3)

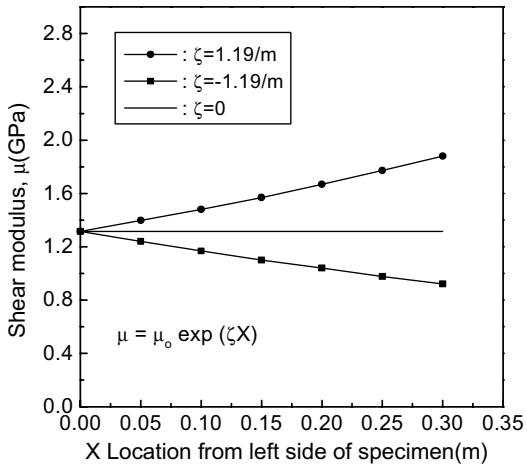

Fig. 2. Variation of shear modulus μ with X location.

variation for a mode II crack. The normalization is carried out by dividing the stress components by $(K/\sqrt{2\pi r})$. In a homogeneous material this would imply that only the singular term of the stress field needs to be considered and due to the normalization scheme the curves for different values of r will fall on top of each other in Figs. 3–8. However, in the case of FGMs, the additional expression of the higher order term $(r^{1/2})$ proportional to the stress intensity factor arising out of nonhomogeneity are still retained through which the nonhomogeneity effects are manifested.

Fig. 3 shows the normalized stress $\sigma_x/\sigma_{\text{I}}^{+}$ around a near stationary crack tip and a propagating crack tip for a value of $\varsigma = 1.19/\text{m}$ under mode I loading. Similar to homogeneous material, for the same value of K_{I}, the normalized σ_x increases with crack propagation velocity and reaches a maximum at $\theta = 0°$ and a minimum at $\theta = \pm 180°$. The stresses very near the crack tip ($r = 0.001$ m) are the same as those for iso-

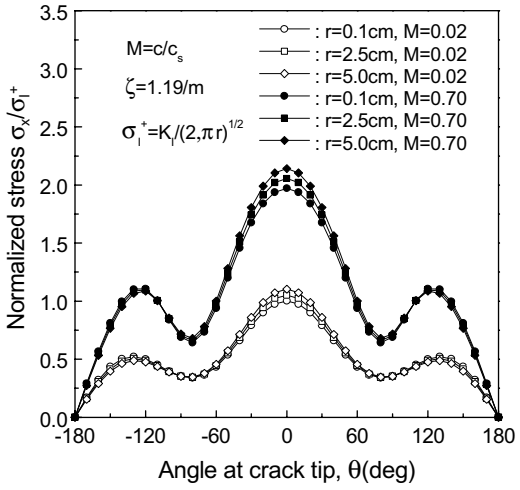

Fig. 3. Normalized stress $\sigma_x/\sigma_{\mathrm{I}}^{+}$ with θ.

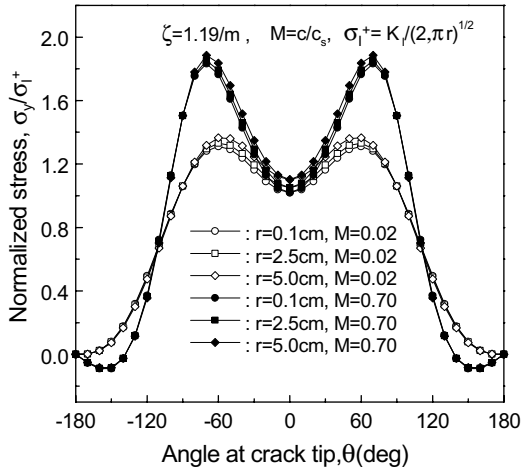

Fig. 4. Normalized stress $\sigma_y/\sigma_{\mathrm{I}}^{+}$ with θ.

tropic materials as this curve coincides with the curve shown for an isotropic material. However, as the values of r increase the curves separate from each other depending on the value of θ, thus, indicating the nonhomogeneity effect. As can be seen from Fig. 3, the effect of nonhomogeneity on stress σ_x is the greatest at $\theta = 0^\circ$ at which the stress in the FGM is greater than that of a homogeneous material. This increase is larger for higher values of r. The results are representative of the increase in mechanical properties along $\theta = 0^\circ$ with increasing r. When the crack is static, σ_x is independent of ς at $\theta = 90^\circ$, when the crack propagates at $M = 0.7$, σ_x is independent of ς at $\theta = 110^\circ$. The result for a static crack is due to the effect of mechanical properties which are constant along $\theta = 90^\circ$, but the result for a propagating crack is due to the effect of mechanical properties as well as crack velocity. σ_x approaches zero on the crack faces and therefore the stress σ_x in this zone is small, nearly the same as that in isotropic materials.

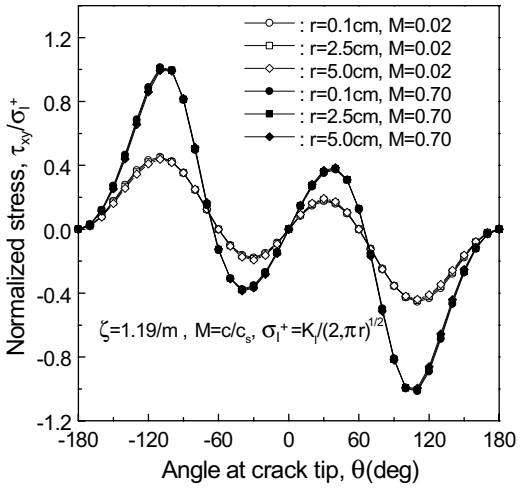

Fig. 5. Normalized stress $\tau_{xy}/\sigma_{\mathrm{I}}^{+}$ with θ.

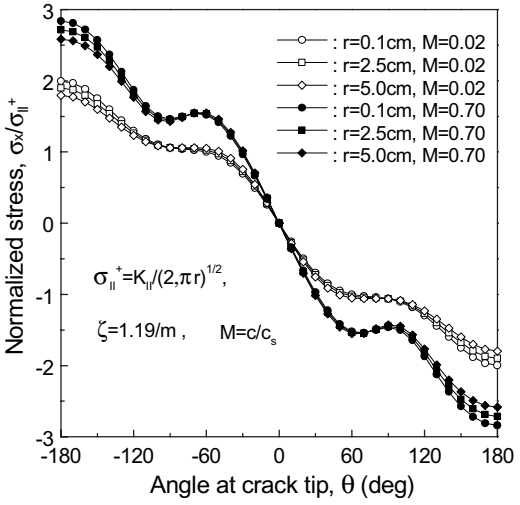

Fig. 6. Normalized stress $\sigma_x/\sigma_{\mathrm{II}}^{+}$ with θ.

Fig. 4 shows the normalized stress $\sigma_y/\sigma_{\mathrm{I}}^{+}$ around stationary and propagating crack tip under mode I loading. In this case, $\sigma_y/\sigma_{\mathrm{I}}^{+}$ is maximum at $\theta = 60°$ when $M = 0.02$, where as for $M = 0.7$ the maximum occurs at $\theta = 70°$. The effect of nonhomogeniety ς on stress σ_y is more significant for $|\theta| \leqslant 80°$ with the greatest at $\theta = 0°$. Similar to σ_x the stress σ_y in FGM is greater than that of an isotropic material as r increases. σ_y is almost independent of ς in the region $90° \leqslant |\theta| \leqslant 180°$ regardless of crack velocity.

The angular variation of the normalized stress $\tau_{xy}/\sigma_{\mathrm{I}}^{+}$ around the crack tip for mode I loading, shown in Fig. 5, indicates that nonhomogeneity has very little effect on shear stress τ_{xy}. The shear stress reaches a maximum at $\theta = 110°$ and is zero along $\theta = 0°$, and $\theta = \pm 180°$ regardless of crack velocity.

The angular variation of the normalized stress components $\sigma_{ij}/\sigma_{\mathrm{II}}^{+}$ for different values of r are shown in Figs. 6–8 for a shear mode crack. In the case of a mode II crack, the nonhomogeniety effects on σ_x reach a

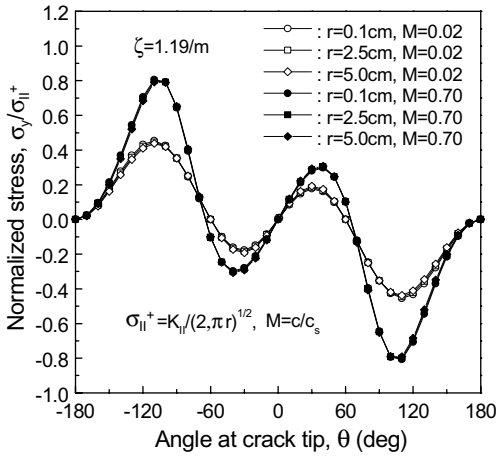

Fig. 7. Normalized stress σ_y/σ_{II}^+ with θ.

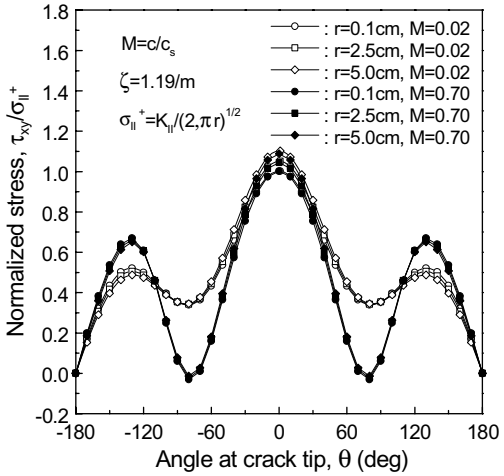

Fig. 8. Normalized stress τ_{xy}/σ_{II}^+ with θ.

maximum at $\theta = 180°$ and increase with increasing r as shown in Fig. 6. In the case of σ_y, the effect of ς is very little as Fig. 5. In the case of shear stress τ_{xy}, the nonhomogeneity effects are dominant around $\theta = 140°$ and $|\theta| \leqslant 60°$, with the maximum effect seen at $\theta = 0°$.

4.2. Isochromatics in FGMs

Isocromatics are generated by the stress optic law (Eq. (42)) combined with stress fields.

$$\sqrt{(\sigma_x - \sigma_y)^2 + 4\tau_{xy}^2} = \frac{Nf_\sigma}{h} \tag{42}$$

where N is the fringe order, h the plate thickness and f_σ the material fringe constant.

In generating these contours, the stress intensity factor K_I and K_{II} were set to 1.0 MPa $\sqrt{m}$ and 0.5 MPa $\sqrt{m}$, respectively, and a material fringe constant f of 6500 N/m-fringe and thickness of $h = 9.5$ mm were assumed. The remote stress in the x direction σ_{ox} was set to zero.

Fig. 9 shows the opening mode isochromatics for a homogeneous material ($\varsigma = 0$) and for two values of ς around a stationary crack tip. One can observe from the contours shown in Fig. 9 that the fringes for a homogeneous material are upright. However, the contours for nonhomogeneous materials, due to non-homogeneity away from the crack tip, tilt away or towards the crack face depending on the sign of ς. When $\varsigma > 0$ (the modulus increases ahead of the crack), the fringes tilt forward whereas for $\varsigma < 0$, the fringes tilts backward. The tilt is more predominant away from the crack-tip. As r approaches 0, the fringes regain their classical form (upright), indicating that the stress components in an FGM are the same as that in isotropic materials only very close to the crack tip.

Fig. 10 shows the isochromatic fringe patterns for a propagating crack tip ($M = 0.7$) for the same value of K used to generate Fig. 9. Generally isochromatic fringes for fast propagating cracks tilt more towards the crack face (backward) compared to those for a stationary crack. As shown in Fig. 10, the backward tilt of the fringe patterns for a propagating crack is greater when $\varsigma < 0$ compared to that when $\varsigma > 0$. This is because the forward tilt due to a positive ς compensates for a portion of the backward tilt due to the crack speed.

Fig. 11 shows the shear mode isochromatic fringe patterns for a stationary crack in an FGM generated using a $K_{II} = 0.5$ MPa $\sqrt{m}$. When the FGM constant ς is zero, the fringes are symmetrical about the y axis. However, when the FGM constant $\varsigma > 0$, the fringes enlarge forward, whereas when FGM constant $\varsigma < 0$,

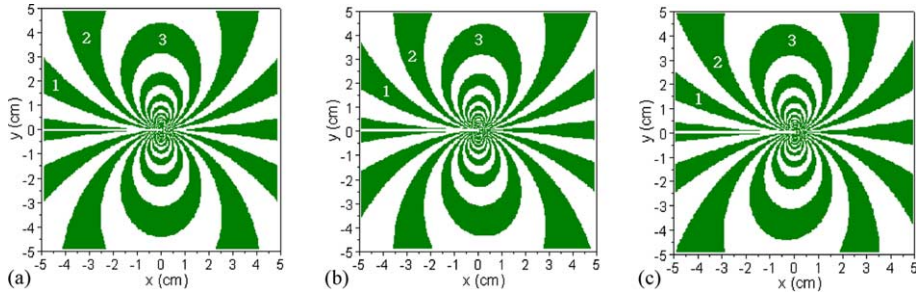

Fig. 9. Isochromatic fringe patterns obtained for a static crack tip in an exponential variation of elastic and physical properties under $K_I = 1.0$ MPa $\sqrt{m}$, $f = 6.5$ kN/m, $h = 9.5$ mm and σ_{x2} (σ_{ox}) = 0. (a) $\varsigma = 0$, $M = 0.02$; (b) $\varsigma = 1.19$, $M = 0.02$; (c) $\varsigma = -1.19$, $M = 0.02$.

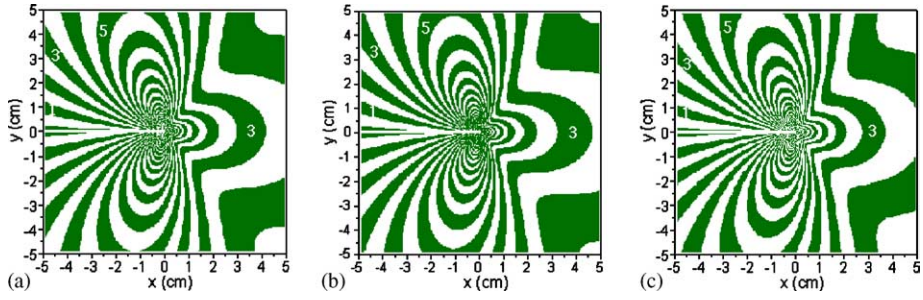

Fig. 10. Isochromatic fringe patterns obtained for a propagating crack tip in an exponential variation of elastic and physical properties under $K_I = 1.0$ MPa $\sqrt{m}$, $f = 6.5$ kN/m. (a) $\varsigma = 0$, $M = 0.7$; (b) $\varsigma = 1.19$, $M = 0.7$; (c) $\varsigma = -1.19$, $M = 0.7$.

the fringe enlarges backward. The results are representative of the fact that the shear modulus increases in the $+x$ direction when $\varsigma > 0$ and decreases in the $-x$ direction when $\varsigma < 0$.

Fig. 12 shows the isochromatic fringe patterns for the propagating crack tip with $M = 0.7$ for the same K_{II}. Similar to Fig. 11, the fringes enlarge more backward when $\varsigma < 0$ compared to that for $\varsigma > 0$.

Fig. 13(a) and (b) shows the opening mode isochromatic fringe patterns for a linear variation of elastic properties with a constant density for the same value of K used to generate Fig. 9. Considering crack length

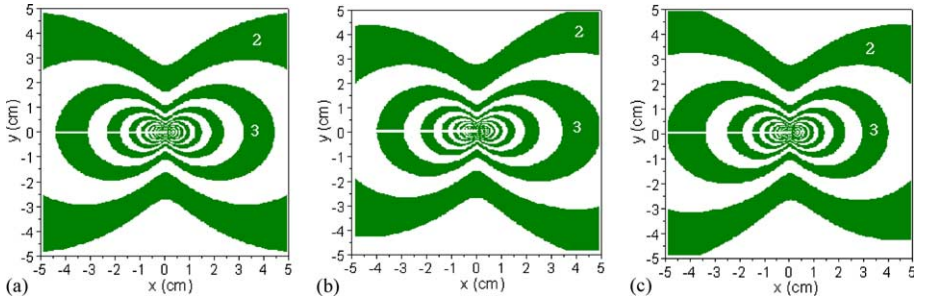

Fig. 11. Isochromatic fringe patterns obtained for a static crack tip in an exponential variation of elastic and physical properties under $K_{II} = 0.5$ MPa $\sqrt{m}$, $f = 6.5$ kN/m. (a) $\varsigma = 0$, $M = 0.02$; (b) $\varsigma = 1.19$, $M = 0.02$; (c) $\varsigma = -1.19$, $M = 0.02$.

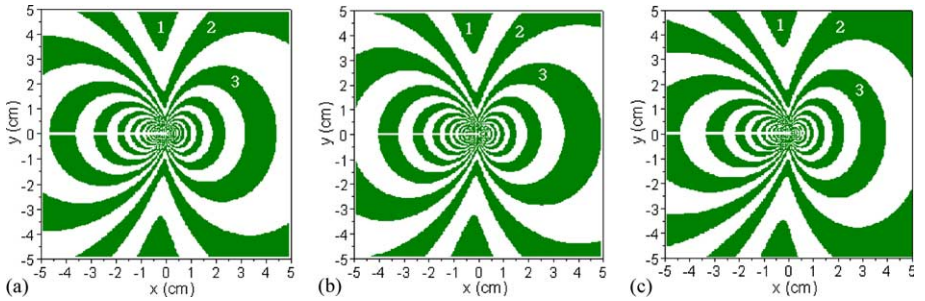

Fig. 12. Isochromatic fringe patterns obtained for a propagating crack tip in an exponential variation of elastic and physical properties under $K_{II} = 0.5$ MPa $\sqrt{m}$, $f = 6.5$ kN/m. (a) $\varsigma = 0$, $M = 0.7$; (b) $\varsigma = 1.19$, $M = 0.7$; (c) $\varsigma = -1.19$, $M = 0.7$.

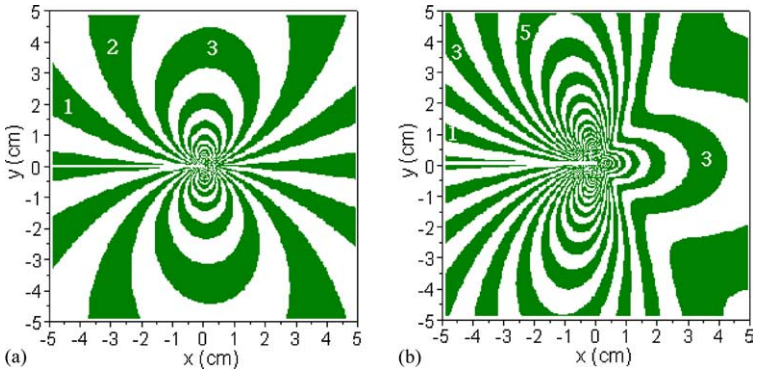

Fig. 13. Isochromatic fringe patterns obtained for crack tip in a linear variation of elastic and properties with constant density. (a) $\varsigma = 1.22$, $M = 0.02$; (b) $\varsigma = 1.22$, $M = 0.7$.

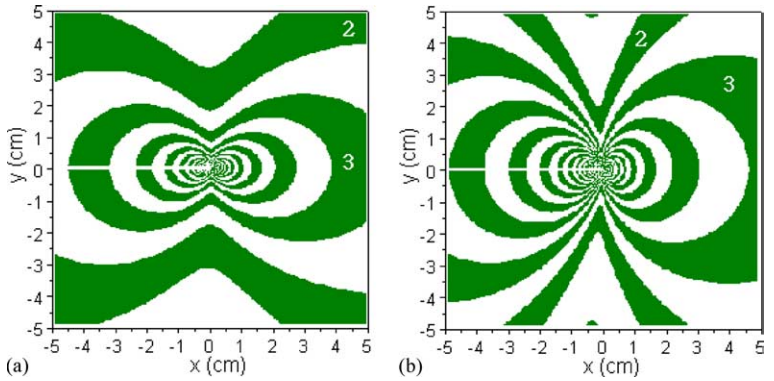

Fig. 14. Isochromatic fringe patterns obtained for crack tip in a linear variation of elastic and properties with constant density. (a) $\varsigma = 1.22$, $M = 0.02$; (b) $\varsigma = 1.22$, $M = 0.7$.

$a = 0.05$ m, the FGM constant ς for the linear variation of elastic properties when $\mu(X) = 1.316(1 + \varsigma X)$ is $1.22/m$, unlike $1.19/m$ for the exponential variation. Comparing Figs. 9 and 13 for stationary crack, the two isochromatic fringe patterns are almost the same. For a propagating crack with $M = 0.7$, the isochromatic fringes for the linear variation of elastic properties with constant density are also nearly the same as those for the exponential variation of properties and density in $-5 < x < 2$ cm, but they are somewhat different for $x > 2$ cm.

Fig. 14(a) and (b) show shear mode isochromatic fringe patterns for linear variations in elastic properties under a constant density for the same values of K used to generate Fig. 11. Comparing Figs. 11 and 14, the isochromatic fringes for the linear variation of elastic properties with constant density are somewhat greater than those for the exponential variation of properties and density.

5. Summary of results

In the study, stress and displacement fields close to a propagating crack tip in an FGM which has (1) a linear variation of shear modulus with constant density and Poisson's ratio, and (2) an exponential variation of shear modulus and density under constant Poisson's ratio, are developed. Experimental methods used in fracture investigations employ such descriptions of the stress field to extract the stress intensity factor from full-filed experimental data sampled from a region between the near field and far field. In this intermediate region, a singular term and one or two higher order terms are sufficient to accurately describe the stress field.

The analysis presented here indicates that at least three terms must be considered in the case of FGM in order to explicitly account for the nonhomogeneity effects. The explicit form of the nonhomogeneity specific higher order terms is developed for FGMs using which the characteristics of the stress fields and the effect of nonhomogeniety on their structure is brought out. The results indicate that nonhomogeniety effects depend on the angular position of the point considered. The effects are dominant in the region around the crack-tip from where experimental data is usually sampled, and hence, the nonhomogeneity specific terms presented here must be included to obtain meaningful estimates of fracture parameters from experimental data.

Appendix A

Let complex variable z put as follows

$$z = x + my \tag{A.1}$$

where m is a variable dependent on crack propagation velocity and physical properties.

Substituting Eq. (A.1) into Eq. (4) transformed with moving coordinates when $\varsigma = 0$, we obtain Eq. (A.2).

$$\begin{aligned} &A(m)\Phi_1''' + mB(m)\Psi_1''' = 0 \\ &mA(m)\Phi_1''' - B(m)\Psi_1''' = 0 \end{aligned} \tag{A.2}$$

where

$$A(m) = \mu_0(k+2)\left[(m^2+1) - \frac{\rho c^2}{\mu_0(k+2)}\right], \quad B(m) = \mu_0\left[(m^2+1) - \frac{\rho c^2}{\mu_0}\right]$$

The characteristic equation of Eq. (A.2) is as follows

$$(m^2+1)\left[m^2 + \left(1 - \frac{\rho c^2}{\mu_0(k+2)}\right)\right]\left[m^2 + \left(1 - \frac{\rho c^2}{\mu_0}\right)\right] = 0 \tag{A.3}$$

The characteristic roots of positive number for the equation are as follows

$$m = \mathrm{i}, \quad m = \mathrm{i}\alpha_\mathrm{l}, \quad m = \mathrm{i}\alpha_\mathrm{s} \tag{A.4}$$

where, the root $m = \mathrm{i}$ is independent of crack velocity and physical properties, it is only depend on relation between $\Phi_1'''(\alpha_\mathrm{l})$ and $\Psi_1'''(\alpha_\mathrm{s})$. Thus, the coefficients of $\Phi_1'''(\alpha_\mathrm{l})$ and $\Psi_1'''(\alpha_\mathrm{s})$ in Eq. (A.2) are as follows.

$$m = \mathrm{i}, \quad A(m) = A(\mathrm{i}\alpha_\mathrm{l}), \quad B(m) = B(\mathrm{i}\alpha_\mathrm{s}) \tag{A.5}$$

Considering $\Phi_1'''(\alpha_\mathrm{l}) = \frac{\partial}{\partial\eta_1}\Phi_1''(\alpha_\mathrm{l})$, $m\Psi_1'''(\alpha_\mathrm{s}) = \frac{\partial}{\partial\eta_2}\Psi_1''(\alpha_\mathrm{s})$ and substituting Eq. (A.5) into Eq. (A.2) integrated with z, we can obtain the relation between $\Phi_1(\alpha_\mathrm{l})$ and $\Psi_1(\alpha_\mathrm{s})$.

$$\frac{\partial}{\partial\eta_2}\Psi_1(z_\mathrm{s}) = -\frac{A(m \to \mathrm{i}\alpha_\mathrm{l})}{B(m \to \mathrm{i}\alpha_\mathrm{s})}\frac{\partial}{\partial\eta_1}\Phi_1(z_\mathrm{l}) = -(k+2)\frac{\partial}{\partial\eta_1}\Phi_1(z_\mathrm{l}) \tag{A.6}$$

$$\frac{1}{k+2}\frac{\partial}{\partial\eta_1}\Psi_1(z_\mathrm{s}) = \frac{\partial}{\partial\eta_2}\Phi_1(z_\mathrm{l}) \tag{A.7}$$

where integral constants related to rigid displacement are ignored.

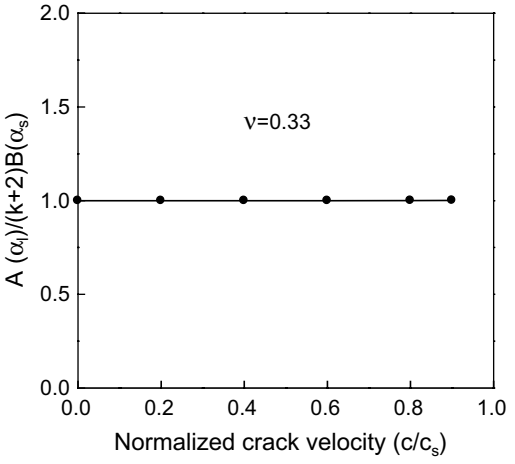

Fig. 15. $A(\alpha_\mathrm{l})/[(k+2)B(\alpha_\mathrm{s})]$ with crack propagation velocity.

We can confirm the $A(\alpha_l)/B(\alpha_s) = k + 2$ in Fig. 15 which obtained under subsonic crack velocity when $v = 0.33$.

References

Atkinson, C., List, R.D., 1978. Steady state crack propagation into media with spatially varying elastic properties. Int. J. Eng. Sci. 16, 717–730.

Butcher, R.J., Rousseau, C.E., Tippur, H.V., 1999. A functionally graded particulate composite: preparation, measurements, failure analysis. Acta Mater. 47 (1), 259–268.

Eischen, J.W., 1987. Fracture of nonhomogeneous materials. Int. J. Fract. 34 (3), 3–22.

Erdogan, F., 1995. Fracture mechanics of functionally graded materials. Compos. Eng. 5 (7), 753–770.

Freund, L.B., 1990. Dynamic Fracture Mechanics. Cambridge University Press, Cambridge.

Gu, P., Dao, M., Asaro, R.J., 1999. A simplified method for calculating the crack-tip field of functionary graded materials using the domain integrials. J. Appl. Mech. 66, 101–108.

Jedamzik, R., Neubrand, A., Rodel, J., 2000. Production of functionally graded materials from electrochemically modified carbon preforms. J. Am. Ceram. Soc. 83 (4), 983–985.

Jiang, L.Y., Wang, X.D., 2002. On the dynamic crack propagation in an interphase with spatially varying elastic properties under inplane loading. Int. J. Fract. 114, 225–244.

Jin, Z.H., Batra, R.C., 1996. Some basic fracture mechanics concept in functionally graded materials. J. Mech. Phys. Solids 44 (8), 1221–1235.

Niino, M., Hirai, T., Watanabe, R., 1987. The functionally gradient. J. Jpn. Soc. Compos. Mater. 13 (1), 257.

Parameswaran, V., Shukla, A., 1999. Crack-tip stress fields for dynamic fracture in functionally gradient materials. Mech. Mater. 31, 579–596.

Parameswaran, V., Shukla, A., 2000. Processing and characterization of a model functionally gradient material. J. Mater. Sci. 35, 21–29.

Parameswaran, V., Shukla, A., 2002. Asymptotic stress fields for stationary cracks along the gradient in functionally graded materials. J. Appl. Mech. 69, 240–243.

Rousseau, C.-E., Tippur, H.V., 2001. Dynamic fracture of compositionally graded materials with cracks along the elastic gradient experiments and analysis. Mech. Mater. 33, 403–421.

Wang, X.D., Meguid, S.A., 1995. On the dynamic crack propagation in an interface with spatially varying elastic properties. Int. J. Fract. 69, 87–99.

Zeng, Y.P., Jiang, D.L., Watanabe, T., 2000. Fabrication and properties of tape-cast laminated and functionally gradient alumina-titanium carbide materials. J. Am. Ceram. Soc. 83 (12), 2999–3003.